We are IntechOpen,
the world's leading publisher of Open Access books
Built by scientists, for scientists

6,900
Open access books available

186,000
International authors and editors

200M
Downloads

154
Countries delivered to

Our authors are among the

TOP 1%
most cited scientists

12.2%
Contributors from top 500 universities

CLARIVATE ANALYTICS
BOOK CITATION INDEX
INDEXED

WEB OF SCIENCE™

Selection of our books indexed in the Book Citation Index
in Web of Science™ Core Collection (BKCI)

Interested in publishing with us?
Contact book.department@intechopen.com

Numbers displayed above are based on latest data collected.
For more information visit www.intechopen.com

Chapter

A Review: Solder Joint Cracks at Sn-Bi58 Solder ACFs Joints

Shuye Zhang, Tiesong Lin, Peng He and Kyung-Wook Paik

Abstract

In this chapter, solder joint cracks at Sn-Bi58 solder ACF joints were investigated in conventional thermal compression bonding and ultrasonic bonding. It was found that resin storage modulus is the crucial for solder joint morphology regardless of bonding pressures. At high temperature, polymer resin tends to rebound above Tg and break the molten solder morphology. We proposed two useful methods to keep off solder joints cracks during bonding process. One is to remain bonding pressure until room temperature, the other is to use fillers to increase resin thermal mechanical property. The thermal cycling reliability was significantly enhanced when solder joint morphology was modified using 10 wt% 0.2 μm SiO_2 fillers in acrylic based Sn-Bi58 solder ACF joints.

Keywords: solder cracks, ACF assembly, flex-on-board assembly, high reliability

1. Introduction

In 2013, Google Company had launched Google Glass, which the first-generation of wearable electronics in the history of humans [1]. Apart from the limited packaging sizes, high-density packaging technologies are demand for chips, passive components, and printed circuit boards. Several functions such as cameras, global positioning system (GPS), wireless communication, touch screen, FM radio, Audio, are also featured in Google Glass [2]. Generally, socket-type connectors have been used to connect between a flexible printed circuit (FPC) module and the main board of Google Glass [3], on the purpose of electrical interconnect. Flex-on-board (FOB) is one type of flip-chip technologies, to assembly printed circuits board (PCB) and FPC using anisotropic conductive films (ACFs) [4].

Aiming at replacing the socket-connectors, FOB assembly is attracting more and more attention, due to a lower thickness (about 50 μm) and a higher fine-pitch capability (under 100 μm) [5]. So Google started to use FOB in mother board assembly to partly take place of connectors, as shown in **Figure 1**. ACFs are usually to be as the interconnection materials to assembly FOB, consisting of thermosetting polymer adhesive matrix and conductive balls [6]. Adhesives will be cured by temperature and functional group will be cross-linked, resulting into the mechanical connection to PCB board and metal pad surfaces [7]. Current flows through an ACF joint formed by a physical contact between electrodes and conductive balls (such as Au/Ni metal balls or Au/Ni coated polymer balls) [8].

Figure 2 shows an Au/Ni metal ACF joint and a Sn based metallurgical ACF joint in a cross-section view using a scanning electron microscope. Compared with
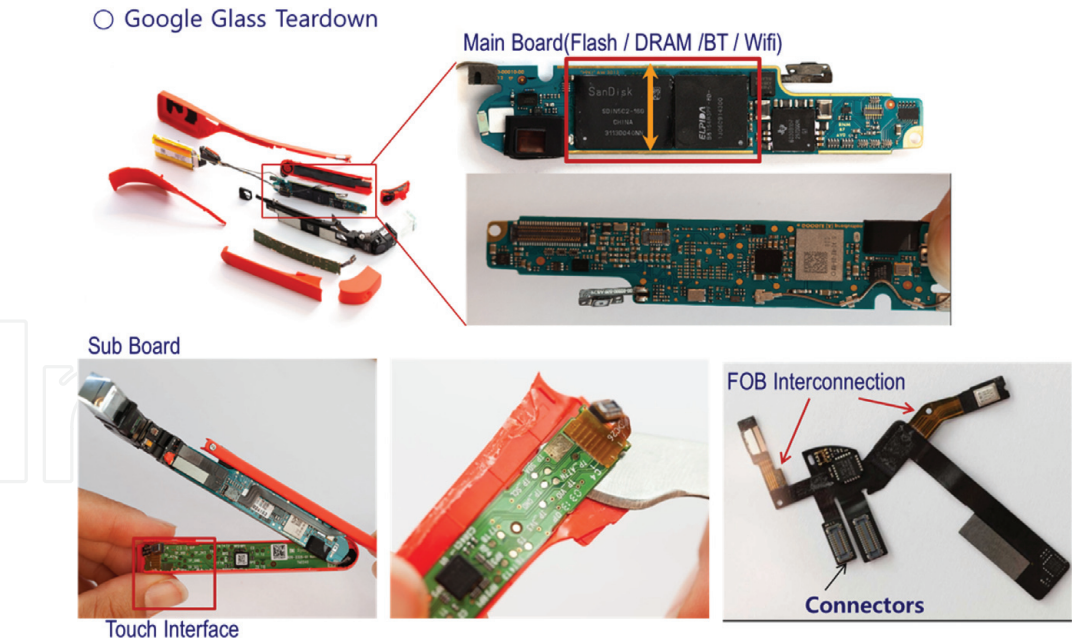
Figure 1.
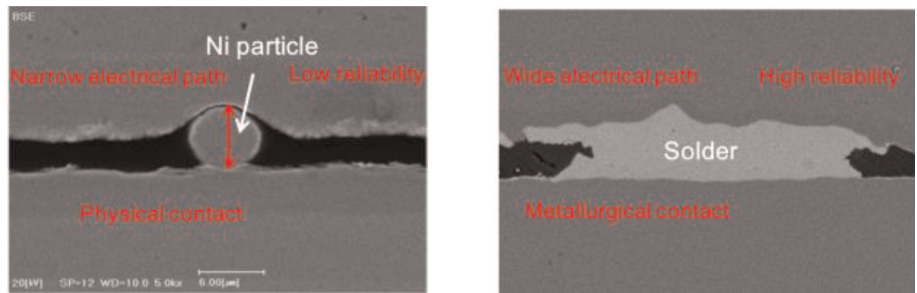*Google glass teardown and FOB interconnection.*

Figure 2.
A comparison of the conventional Ni and Sn solder metallurgical anisotropic conductive films (ACFs) joints.

a metal ACF joint, high contact resistance, poor power handling capacity and reliability can be improved by using solder metallurgical ACF joint, due to wide electrical paths and stable metallurgical interconnection [9, 10]. In order to remove solder oxide layer and improve solder wettability, two methods, a thermal compression (TC) bonding combining a flux material [11] and an ultrasonic (US) bonding without flux materials [12], are used. According to previous results, the heating rates were raised rapidly to 400°C/s and the temperature of solder ACF joints reached above 250°C under US vibration. By adjusting various ultrasonic amplitudes of vibration (from 4 to 13 μm), the ACF temperature could be precisely controlled from 70 to 250°C.

A perfect solder ACF joint morphology containing a Sn–3Ag–0.5Cu (SAC305) alloy has been optimized by using lower viscosity, faster curing speed, higher resin property based cationic epoxies with high elastic modulus on a 250°C bonding temperature for FOB assembly [13]. Low viscosity helps resin flow during bonding process [14] and faster curing speed indicates higher cross-linking density and mechanical property of polymer resins [15]. Compared with acrylic resin, imidazole resin and multifunctional epoxy enhanced imidazole resin, cationic epoxy resin has the highest elastic modulus when it is fully cured, therefore, few solder joint cracks are taken place at ACF joints after FOB assembly. Not only resin property is a basic issue, bonding time also plays an important role in solder joint morphologies, especially for cracks [16]. Since micron sized solder ACF joint is so tiny that Sn

elements quickly diffused into Au/Ni metal surface to form brittle intermetallic compound (IMC), cracks were formed by the residual Bi phase and the newly formed IMC phases. As a result, 10 seconds bonding time was optimized to avoid over-diffusion behavior of Sn elements at micron solder ACF joints.

At optimized 10 seconds bonding time, depending on their solder melting temperatures, SAC305 (221°C) and Sn-58Bi (139°C) solder ACFs are bonded at 250 and 200°C joint temperatures, respectively. For those resins with high elastic modulus (such as imidazole resin, multifunctional epoxy enhanced imidazole resin, and cationic epoxy resin), solder cracks were rarely found at ACF joints after TC assembly in FOB interconnection. On the contrary, for these resins with low elastic modulus (such as acrylic resin), solder joint crack was a critical issue after FOB assembly [17]. Although bonding temperature was suggested not higher than 220°C for acrylic ACF resins to avoid thermal decomposition and solder joint cracks, solder joint cracks were even observed at low modulus based acrylic resin joints at 200°C bonding temperatures.

Although polymer rebound of the cured acrylic resin had been measured as approximate 1–3% dimension change of polymer resin, when the bonding pressure was released at 200°C bonding temperature [17]. In this chapter, we aimed at finding out the obvious inner factor of polymer resins to determine Sn-58Bi solder cracks after FOB assembly at acrylic ACF joints, rather than a perfect solder joint morphology using other ACF resins. After that, two available throughout methods were discussed to increase acrylic resin elastic modulus to solve solder joint crack after FOB assembly. Moreover, the consequent solder joint morphologies were observed, compared and analyzed. The significance of this research is to guide ultra-low elastic modulus ACF resin assembly to form reliable solder joints for low melting solder materials and electronic device packaging.

2. Experiments

2.1 Test vehicles and materials

Test vehicles was shown in **Figure 3**. FR-4 printed circuit board (PCB) was 1-mm-thick and flexible printed circuit (FPC) board was made by polyimide with 50-μm-thick, and 500-μm-pitch Cu patterns with electroless nickel immersion gold (ENIG) finish were plated on test vehicles.

Three kinds of polymer resins were compared for the ACFs, acrylic resin, imidazole resin and cationic resin. These products were all bought from H&S company in South Korea. About 5 wt% 8-μm-diameter Ni particles, 0.2 μm silica fillers,
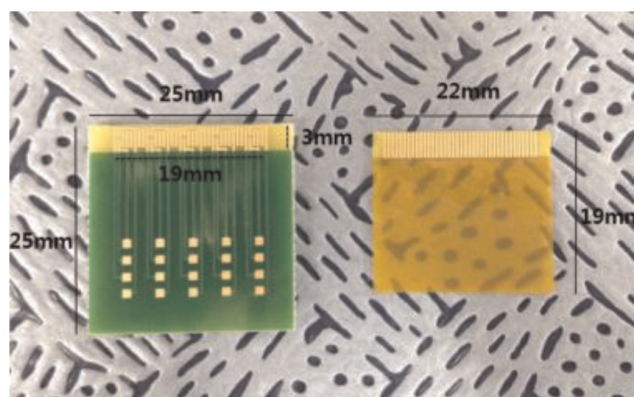

Figure 3.
500-μm-pitch printed circuit board (PCB) and flexible printed circuit (FPC) board.

	Weight percentage			Calculated volume percentage			
Solder ACFs	Sn-58Bi solder (8.56 g/cm^3)	Polymer resin (1.25 g/cm^3)	Ni particle (8.9 g/cm^3)	Silica filler (2.65 g/cm^3)	Sn-58Bi solder (8.56 g/cm^3)	Polymer resin (1.25 g/cm^3)	Ni particles (8.9 g/cm^3)	Silica filler (2.65 g/cm^3)
ACF 1	30%	1	5%	0%	6.25%	92.75%	1%	0%
ACF 2	30%	1	5%	5%	6.1%	89.7%	0.97%	3.23%
ACF 3	30%	1	5%	10%	5.9%	86.9%	0.93%	6.27%

Table 1.
The specification of solder ACFs.

30 wt% 25–32 μm diameters Sn-58Bi particles, and 2 wt% flux material were added in the pure resins and then proceeded the film coating process. After that, 50-film-thickness anisotropic conductive film was achieved. **Table 1** gives the specifications of the added materials, such as weight percentages of the pure polymer resins and the calculated volume percentages of the total ACFs materials with additives.

Molten solder joint was like a water above its melting temperature and squeezed by bonding pressure, resulting into uniform solder joint morphology after bonding [18–20]. Thus, Ni particles were used to obtain uniform joint gap size and control solder joint morphology. Before coating process of ACF, polymer matrixes and conductive particles were stated in a solution. Silica fillers were gradually added as a function of weight percentage by hands [21–23]. Since the solution viscosity was be very high when adding the nano-size solid silica fillers, plenty of toluene would be added to decrease the solution viscosity and make sufficient dissolution between nano sized silica fillers and polymer matrixes. In addition, considering the agglomeration of nano size silica fillers, a magnetic stirring apparatus was carried out at 30°C for 0.5 hour and then a rolling mechanical stirring was performed at room temperature for 12 hours. As a result, a sufficient dissolution between nano size silica filler and polymer resin solution was achieved. **Figure 7** shows the fresh ACFs were put on the PCB ENIG metal electrodes before bonding process.

2.2 Bonding methods

2.2.1 Thermo-compression bonding

According to previous results [17], the bonding parameters (peak temperature, time, and pressure) were optimized as 200°C 10 seconds and 1 MPa. **Figure 4** gives a heat conduction mechanism from a hot bar to ACF joint on a FOB application. Thermal setting adhesives were cured due to the heat conduction from the high temperature of hot bar. **Figure 5** shows a clear temperature profile according to previous result, where temperature was quickly up to Sn-58Bi solder melting point (139°C) and then gradually reached the 200°C peak temperature at 4 seconds. Afterwards, solder ACF joint temperature was remained at 200°C from the 4th to 10th second, and then solder ACF joint entered cooling procedure without any pressure protect.

However, it showed solder joint temperature reached 139°C in the cooling process until 11th second, which means from 10th to 11th second solder ACF joint freely cooled and was not protected with pressure. It is well known that molten solder joint is very weak and its morphology is easy to be destroyed by polymer property, for example, polymer will be rebound on the moment of TC bonding finish and hot bar releasing from test vehicles [24]. Therefore, the mismatch between resin property and molten Sn-58Bi solder property under the cooling
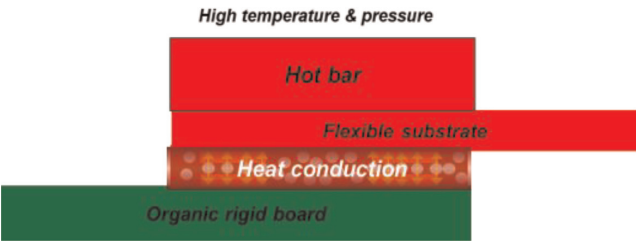
Figure 4.
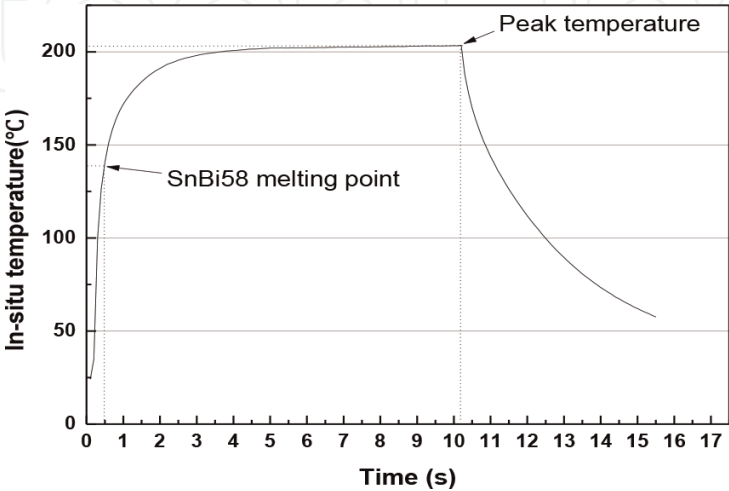*Heat conduction mechanism in a TC bonding.*

Figure 5.
The in-situ temperature profile of solder ACFs joint by a TC bonding.

process should be investigated. At here, in-situ temperature is precisely measured by a K-type thermocouple every 0.1 seconds [25].

2.2.2 Ultrasonic bonding

Figure 6 shows another mechanism of local heat generation by ultrasonic vibration at room temperature. Unlike TC bonding, US bonding was applied at room temperature and bonding pressure can be controlled as a function of time, which means the bonding pressure can be maintained through the whole bonding procedure until ACF joint cooling to room temperature [25]. In this way, ACF adhesives and solder joint were protected under bonding pressure during cooling process, to reduce the influence of heated resin to molten solder joints. During the US bonding, polymer resin can also be cured by the spontaneous ultrasonic vibration at room temperature environment. Compared with TC bonding, the joint temperature was slowly
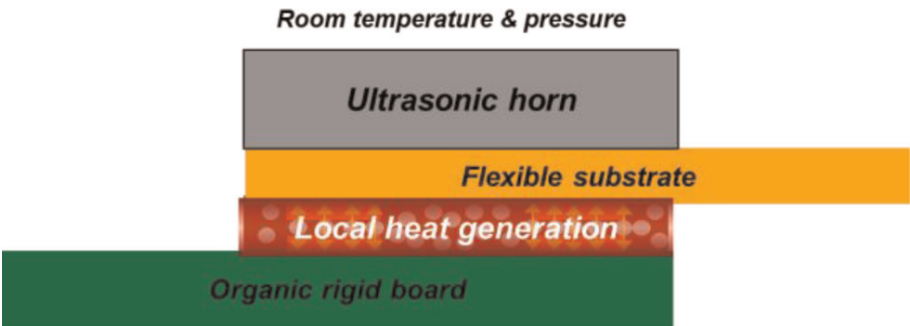

Figure 6.
Mechanism of local heat generation by ultrasonic vibration at room temperature.
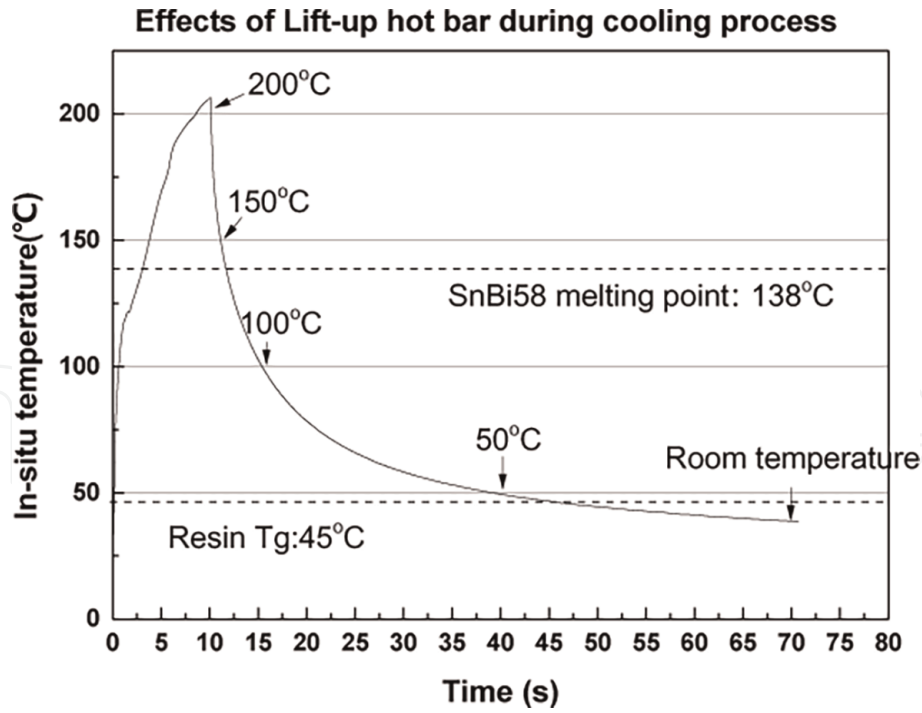
Figure 7.
The in-situ temperature and the designed lift-up time of bonding pressure in US bonding.

increased up to 200°C, however, resin would be fully cured and solder metallurgical joint could be obtained as well [26]. **Figure 7** shows the in-situ ACFs joint temperature and the designed lift-up time of bonding pressure in US bonding. Referring to previous results, polymer rebound amount will be decreased as temperature decreased [17]. At here, we focus whether it is possible to prevent the solder joint damage at a lower temperature releasing bonding pressure during the cooling process.

2.3 Differential scanning calorimetry (DSC)

Many studies have been reported the curing degree of acrylic ACF joints by TC or US bonding using DSC [14, 17, 26, 27]. It has been convinced that acrylic resin can be fully cured at 200°C 10 seconds condition and provide the best thermo-mechanical property after its full cure [28]. Considering there is an exothermic peak from 75 to 150°C caused by acrylic resin cure and a sharp endothermic peak from 135 to 142°C caused by Sn-58Bi solder melting, there might be interplay by two materials and unclear to demonstrate the Sn-58Bi solder melting in the temperature heating-up period. On the other hand, it is important to know the solidification temperature of Sn-58Bi alloy during the temperature cooling-down period. Because mechanical protection of Sn-58Bi alloy will be established when alloy is solidified [29, 30].

Therefore, only pure Sn-58Bi alloy was tested by DSC to obtain the melting and solidification temperature, respectively. In details, Sn-58Bi solder alloy was put by 20 mg weight. The heating rate was 20°C/minutes from 30 to 300°C, afterwards, the temperature was along with furnace cooling to room temperature at a nitrogen environment. The curing behavior of acrylic resin used in this study and curing degree after bonding process measured by a Fourier transform infrared spectroscopy can be found at here [14, 17, 26, 27].

2.4 Thermomechanical analysis

A thermomechanical analyzer (DMA) was used to measure the storage modulus of the cured polymer resin as a function of temperature. The resin film was prepared

by the thickness of 50 μm, the length of 10 mm, and the width of 2.5 mm, and it was cured at the oven environment of 150°C for 3 hours. In DMA environment, resin film was tested under a 0.1 Hz load with a 10 mN dynamic stress, and the static tensile force was prepared by 50 mN. In addition, the DMA environment was heated by 5°C/minutes until 200°C from room temperature. The elastic property of polymer resin in this study was considered in z direction, because the polymer rebound tool place vertically, resulting into the ACF dimension change and solder joint cracks. As Eq. (1) was shown in the following, elastic strain is mathematically determined by the ratio of length change (ΔL) over the initial ACF length (L). The larger changed length of polymer resin by DMA force indicates the larger polymer rebound when bonding tool was disappeared. In addition, the coefficient of thermal expansion (CTE) of adhesives were also measured by a 50 mN tensile force.

$$Strain = (\Delta L)/L \qquad (1)$$

2.5 Joint resistance and morphologies

After bonding process, ACFs joint was formed and its resistance was detected by a contact method, which is called 4-point-probe kelvin method. Referring to Ohm's Law, we have learnt that resistance is mathematically named by the ratio of electrical voltage above its corresponding current. As a constant current was applied through all over the circuit, the resistance of the specific part is easy to know unless the voltage is precisely measured [31].

Actually, a delta mode in KI 6220 nano-voltmeter has been widely used to measure the microscale ohms from the American Keithley company. The constant current was designed and perfectly applied in Cu lines at PCB and FPC substrates, as a result, solder ACFs joints were performed by current, voltage drop by can be measured by KI 6220 m, which was shown as the grown overlapped part in **Figure 8**. For accurately measuring the contact resistance of solder ACF joint, one measurement is repeated by 10 times. In details, Cu pad areas was 0.3 mm^2 and 40 channels were designed in PCB test vehicles.

A scanning electron microscope (SEM) in this paper was utilized to apparently observe the changing of solder ACFs joint morphologies before and after sever cracks. In order to obviously compare Sn and Bi elements in solder joint morphologies, a backscattered electron mode was carried out in SEM environment. For the typical solder morphologies, such as solder joint heights, shapes, and cracks, we performed at SEM images and evaluated them at certain conditions.

2.6 Reliability evaluation

To characterize cracks at solder joint morphologies on the effects of electrical performance, a thermal cycling reliability from −45 to 125°C was tested until 1000 cycles. TC bonded Sn-Bi58 solder ACFs joints with 0, 5, and 10 wt% of 0.2 μm
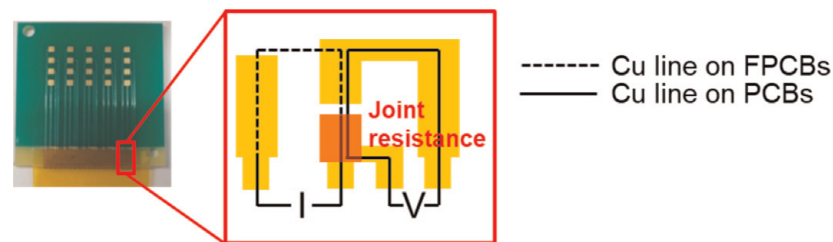

Figure 8.
Electrical design for a four-point-probe measurement.

SiO$_2$ fillers addition were compared in this thermal cycling test. What is more, the dwell time of -45°C was remained for 15 minutes and it rapidly increased to 125°C for 15 minutes dwelling time. Joint contact resistances in this thermal cycling test were designed to be recorded every 200 cycles. Until 1000 cycles, joint morphologies and each failure mode of Sn-Bi58 solder ACF joints with or without silica modified were compared through the observation of SEM images.

3. Results and discussion

3.1 Effects of resin modulus on solder joint cracks

Figure 9 shows the thermal mechanical properties of typical adhesives films as a function of temperatures. Compared with conventional epoxies by imidazole and cationic curing types with higher Tg (over 100°C), acrylic adhesives showed lower modulus, because it was a low Tg material (45°C). Especially at 200°C when hot-bar releasing bonded samples at the end of TC bonding for Sn-58Bi solder ACFs applications, even cured acrylic adhesives showed 0.4 Mpa storage modulus, and cationic epoxy and imidazole epoxy showed 7.1 and 5.7 Mpa, respectively.

Figure 10 shows Sn-58Bi solder ACFs joints cracks using this low Tg and low modulus acrylic adhesives regardless of bonding pressures from 1 to 3 Mpa. However, there are no solder joint cracks when using other higher storage modulus adhesive materials under the same bonding pressures.

In terms of solder joints cracks, there are two assumptions on it: one is CTE mismatch between shrink adhesives and solders during cooling process, the 2nd is higher elasticity of adhesives than molten solders when bonding pressure is removed, and then liquid solder joints are cracked under high temperature.

Figure 11 shows endothermic and exothermic behaviors of Sn-58Bi solder materials in a DSC analysis. In a heating period, Sn-58Bi solder melts at 139°C and stay at a liquid state until cooling to 125°C, and Sn-58Bi solders were totally solid below 90°C. As a result, adhesives shrinkage or rebound is able to cause liquid Sn-58Bi solder joints cracks only above 90°C, because solid Sn-58Bi joint is with 30.9 Gpa young's modulus [32] which cannot be cracked. **Figure 12** gives the thermal expanded behaviors of three typical adhesives. The shrinkage percentages of three adhesives films were summarized in **Table 2** in cooling process. 90°C is lower than the imidazole epoxy's Tg and cation epoxy's Tg, as a result, there was a huge shrinked amount when cooling process was lower than glass transition temperature
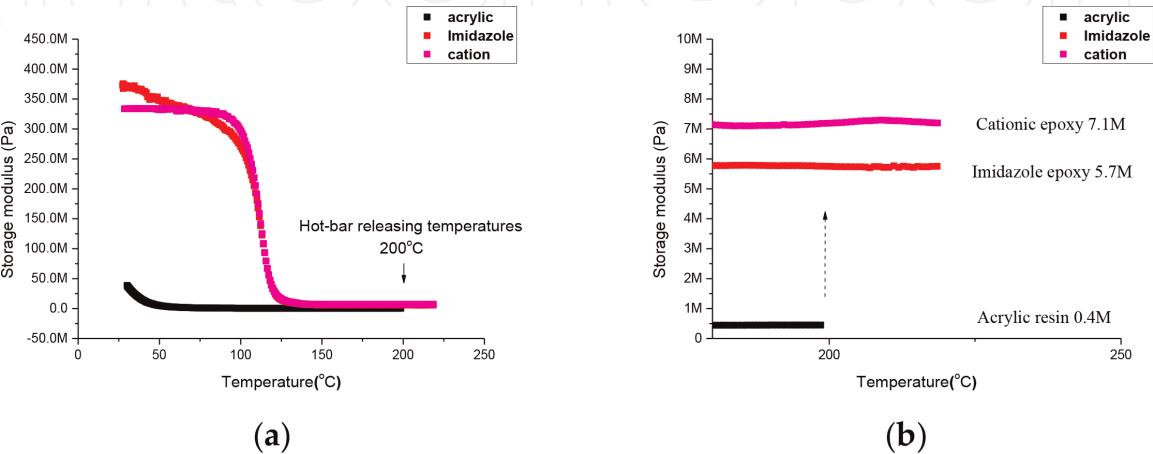

Figure 9.
*Storage modulus of typical adhesives films as function of temperature. (**a**) 30–250°C (**b**) specific region at 200–250°C.*
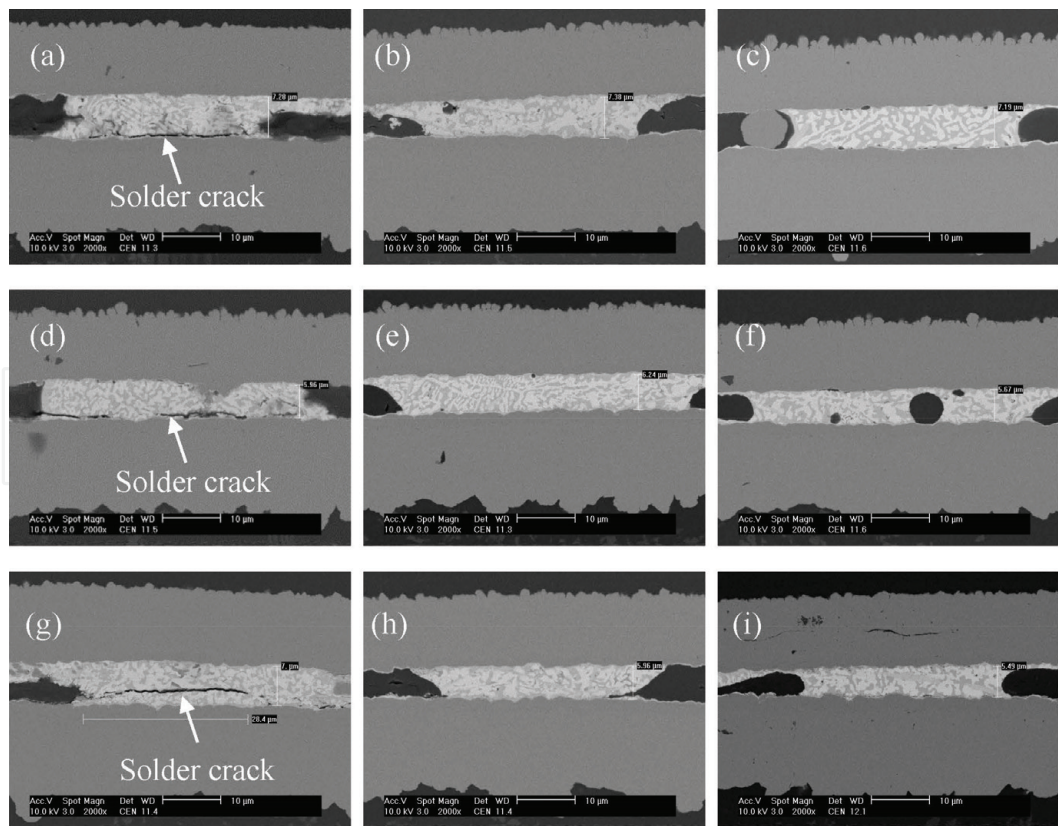
Figure 10.
Solder joint morphologies of Sn-Bi58 ACFs joints by various bonding pressures. (a, d, g) Acrylic resins bonded by 1, 2 and 3 MPa, respectively; (b, e, h) imidazole epoxy bonded by 1, 2 and 3 MPa, respectively; (c, f, i) cationic epoxy bonded by 1, 2 and 3 MPa, respectively.
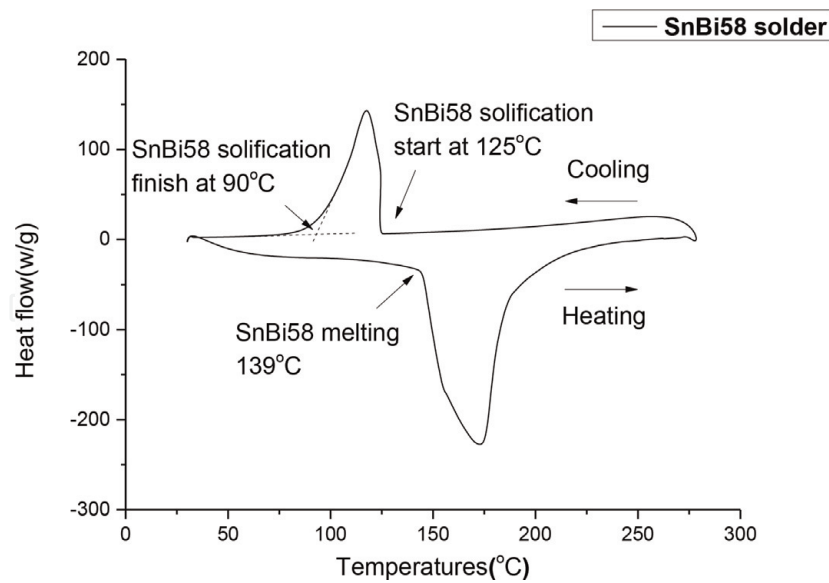

Figure 11.
DSC behaviors of Sn-58Bi solder during heating and cooling process.

at two epoxies. −11.2, −13.2 and −5.2% dimension shrinkage were shown for acrylic resin, imidazole epoxy and cation epoxy in the cooling region from 200 to 90°C. However, good solder joint morphologies were found at imidazole epoxy based Sn-58Bi solder ACFs joints in **Figure 10**. As a result, solder ACFs joint cracks were not related with compressive stress by adhesives shrinkages in the cooling process, but related with resin elasticity, especially for lower modulus acrylic adhesives.
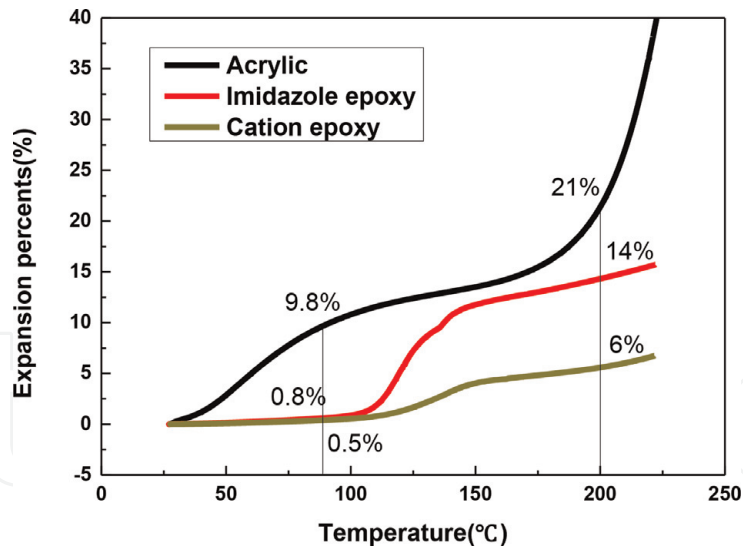
Figure 12.
Thermal expansion properties of typical adhesives films.

Adhesive modulus is divided by storage and loss modulus in viscoelastic materials [33]. Storage modulus is to measure the stored energy and represent the elastic property, and loss modulus is to measure the energy dissipated as heat and represent the viscous property [34]. In this study, solder joint cracks were due to adhesive rebound, which is elastic properties, and not due to heat dissipation and adhesive viscos property, so storage modulus is used.

Figure 13 illustrates the strain changes of acrylic based Sn-58Bi solder ACFs with respect to the 50 mN tensile sinusoidal load with 10 mN amplitude and 0.1 Hz frequency in DMA analysis as a function of temperatures. In details, strain changes in **Figure 13** were consisted of two parts, one part is due to thermal expansion and the other is elastic strain due to plastic deformation. In this study, the plastic deformation, which is the dimension recover of deformed polymer when mechanical loading disappeared, is used to estimate adhesive rebound. According to the following equation, storage modulus is the ratio of applied tensile stress to elastic strain. In other words, adhesive rebound amounts are reversely proportional to its storage modulus in the following Eq. (2).

$$Storage\ modulus = Stress/(Elastic\ strain) \tag{2}$$

Because Tg of acrylic resin is 45°C, adhesive showed a relatively higher modulus at room temperatures below 45°C and lower modulus above 45°C. As a result, the elastic strain is smaller below 45°C and larger at above 45°C. In addition, 30 wt% Sn-58Bi solder particles melting behavior at 139°C will enlarge the measured sample dimension in **Figure 13**. **Figure 14** shows storage modulus of acrylic adhesives were increased during cooling process and **Table 3** summarizes specific storage modulus of acrylic adhesive during cooling process.

Dimension change	Acrylic	Imidazole epoxy	Cation epoxy
200°C	21%	14%	6%
90°C	9.8%	0.8%	0.8
200 Cooling to 90°C	−11.2%	−13.2%	−5.2%

Table 2.
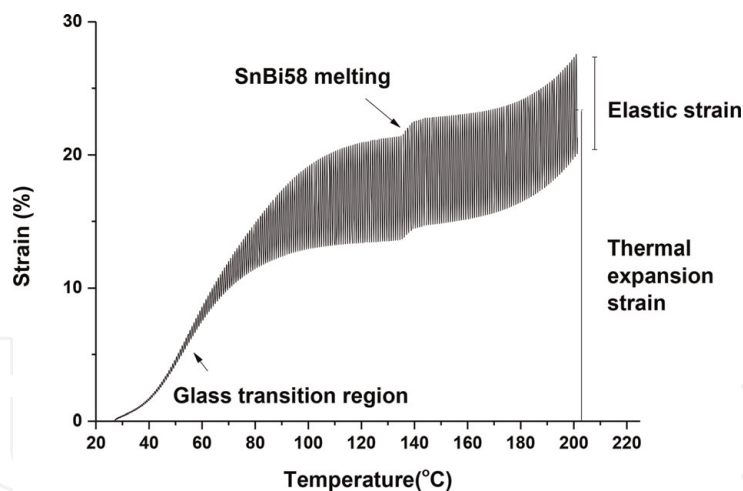*Shrinkage percentages of typical adhesives films during cooling.*

Figure 13.
Strain of acrylic based Sn-58Bi solder ACFs in respect to a sinusoidal load applied in the DMA test as a function of temperatures.

3.2 Effects of US bonding on enhancing resin modulus

Figure 15 shows the effects of delaying ultrasonic horn lift-up time on the acrylic based Sn-58Bi solder ACFs joint morphologies during an US bonding method. A crack-free Sn-58Bi solder ACFs joint can be successfully obtained by maintaining pressure below 45°C the acrylic adhesives Tg during a cooling process, because high storage modulus was established at low temperatures. Because 90°C is the complete point of Sn-58Bi solder joint solidification in **Figure 11**, there was a still solder joint crack when removing bonding pressures at 100°C in **Figure 15**. However, over 30 seconds remaining pressure time is too long for assembly.

3.3 Effects of silica filler on enhancing resin modulus

The faster approach of removing the solder joint crack is to increase resin storage modulus over Tg by adding silica fillers into acrylic polymer resins.
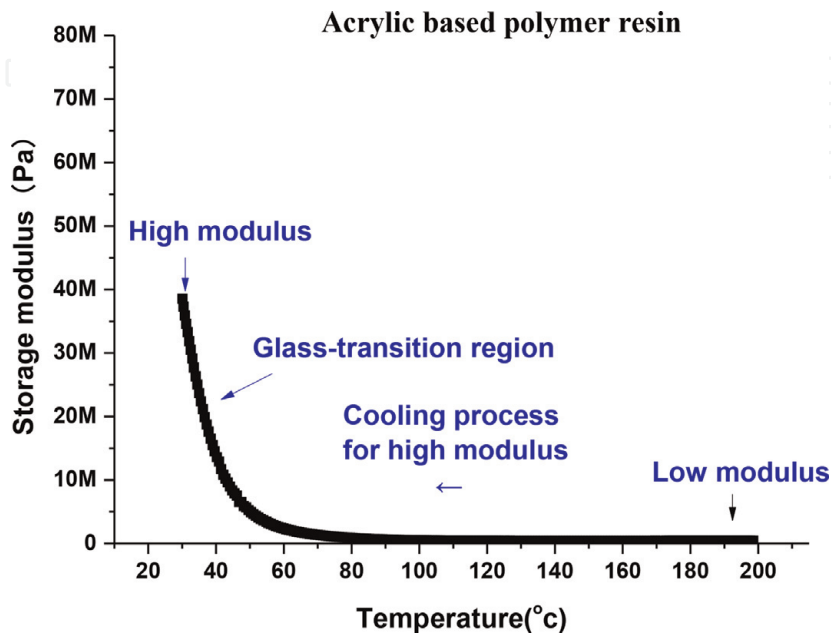

Figure 14.
Increased storage modulus of acrylic solder ACFs during cooling process.

Figure 16 shows the strain amount decrease of acrylic based Sn-58Bi solder ACFs as a function of temperature by adding 0, 5 and 10 wt% of 0.2 μm silica fillers. Both the amount of the thermal expansion and the elastic strain of polymer resin were reduced by adding silica filler. It was known that reducing the thermal expansion strain and the elastic strain as a function of temperatures are good for the joint reliability in T/C test and the good solder joint formation, respectively [35]. Storage modulus of acrylic based Sn-58Bi solder ACFs with addition of 0, 5, and 10 wt% 0.2 μm silica was increased from 0.4 to 0.9 and 1.3 Mpa in **Figure 17**, respectively.

Temperature	200°C	150°C	100°C	50°C	30°C
Modulus	0.4 MPa	0.44 MPa	0.53 MPa	5.2 MPa	34 MPa

Table 3.
Storage modulus of acrylic adhesive during cooling process.
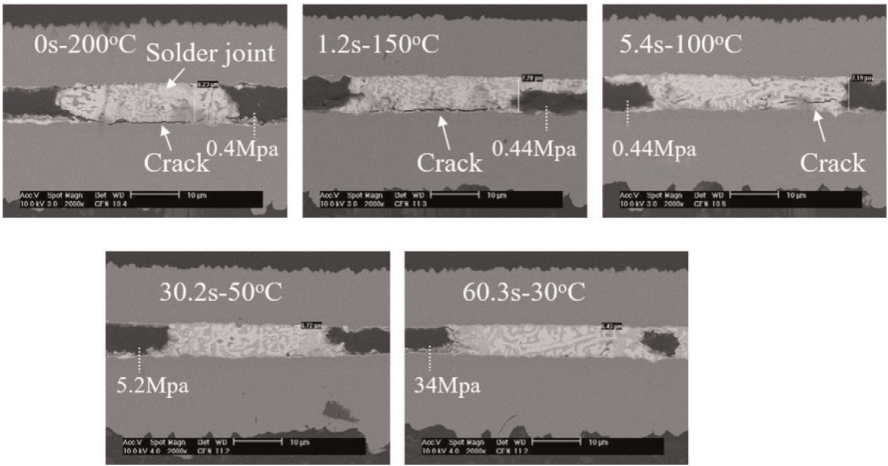

Figure 15.
Effects of delaying ultrasonic horn lift-up times (0, 1.2, 5.4, 30.2, and 60.3 seconds) on the Sn-58Bi solder ACFs joint morphologies.
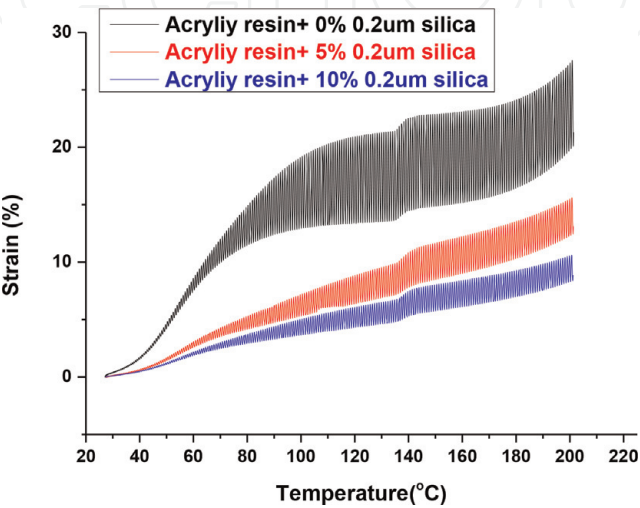

Figure 16.
Strain of acrylic based Sn-58Bi solder ACFs with added silica fillers as a function of temperatures.

3.4 T/C reliability

Figure 18 were listing the solder joint morphologies by adding 0, 5 and 10 wt% 0.2 μm sized silica filler of acrylic based Sn-58Bi solder ACFs joints before and after T/C reliability for 1000 cycles. Referring to the enhancement of elastic modulus by adding several silica fillers in **Figure 17(b)**, solder joint cracks were completely removed for acrylic based Sn-58Bi solder ACF joints at 200°C TC bonding condition with several bonding pressures.

For acrylic based Sn-58Bi solder ACFs without added silica fillers, total joint failure occurred at the interface between Sn-58Bi solder joints and Cu metal electrode after 1000 cycles T/C reliability test, because initial solder joint cracks have already existed before the T/C reliability test. Although elastic modulus was increased double by adding 5 wt% 0.2 μm silica fillers, a small solder crack still remained and propagated at Sn-58Bi solder joints resulting in unstable joint contact resistance during T/C reliability. Excellent solder joint morphology was obtained after the 1000 cycles T/C reliability, because initial solder joint crack was perfectly
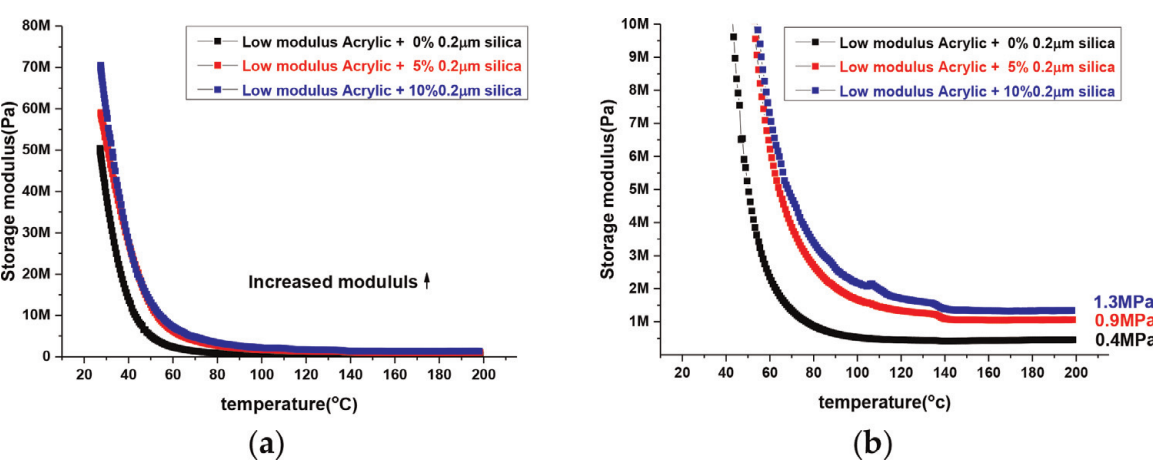
Figure 17.
Elastic modulus of acrylic based Sn-58Bi solder ACFs by adding 0, 5, and 10 wt% 0.2 μm silica fillers at (a) 0–80 MPa and (b) 0–10 MPa ranges.

Figure 18.
Solder joint morphologies of acrylic based Sn-58Bi solder ACFs added by 0, 5, and 10 wt% 0.2 μm silica filler before and after 1000 cycles reliability test.
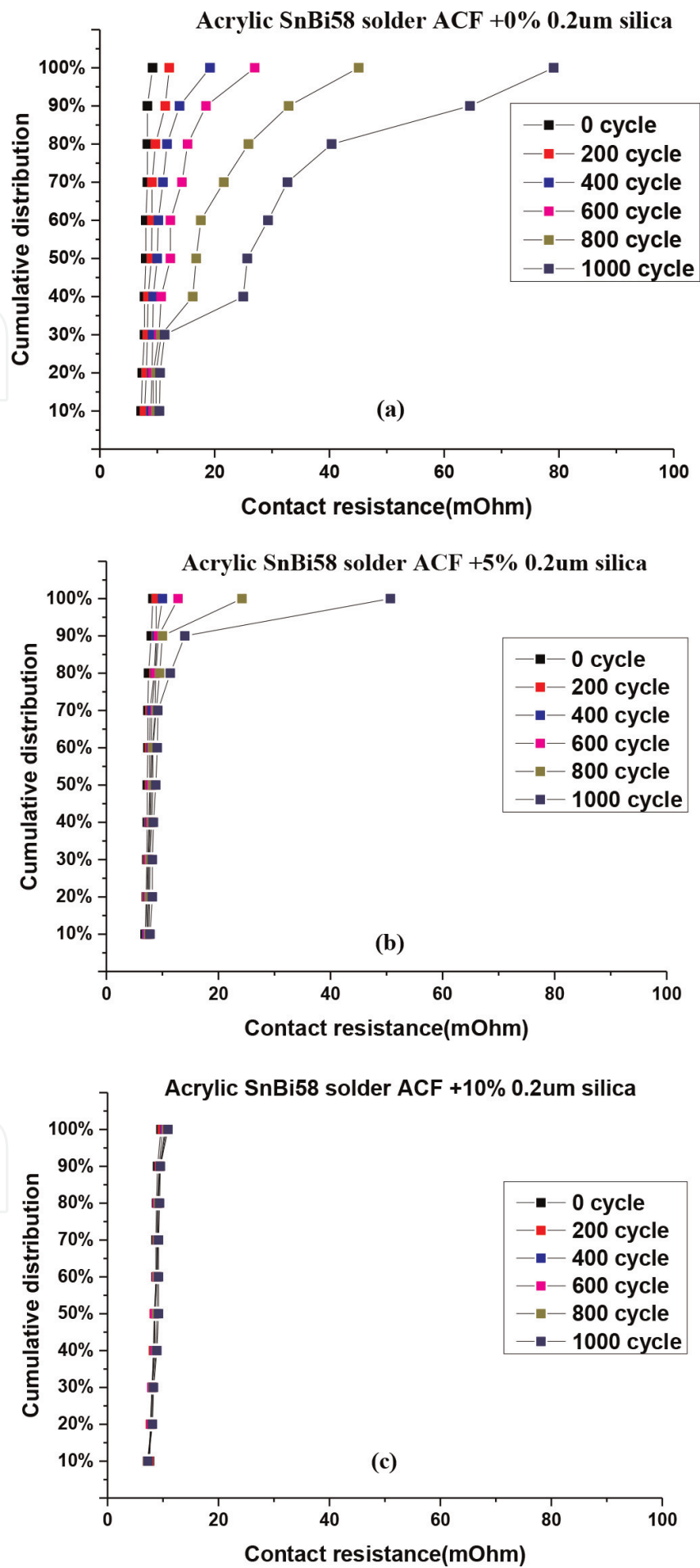
Figure 19.
*Solder joint contact resistances of acrylic based Sn-58Bi solder ACFs up to 1000 cycles T/C reliability as a function of (**a**) 0, (**b**) 5, and (**c**) 10 wt% 0.2 µm silica fillers addition.*

removed at Sn-58Bi solder ACF joints by adding 10 wt% 0.2 µm silica fillers. **Figure 19** shows the 1000 cycles T/C reliability results in terms of contact resistance, and stable joint contact resistance was achieved by adding 10 wt% 0.2 µm silica fillers due to crack-free solder joint.

4. Conclusion(s)

In this paper, we investigated the resin properties and bonding parameters on the solder joint morphologies of Sn-Bi58 ACF joints. As a result, we found storage modulus of resin adhesives was the determined factor for solder joint cracks and regardless of bonding pressures. We thought cracks at solder joints happened, probably due to the high elasticity of polymer resin. Apart from that, two suggestions were listed to solve the solder joint cracks by increasing the resin storage modulus. The 1st one was to remain the hot-bar until cooling to its Tg, but this method will excessively consume solder and lead to brittle IMC at interfaces in TC bonding, while it is ok to US bonding. The other method was to add silica fillers in polymer resin to increase its thermos-mechanical property and reduce the polymer rebound when bonding process was finished. For ultrasonic bonding, storage modulus above 5 MPa of was at least needed to prevent solder joint cracks. On the contrast, 70 seconds for maintaining bonding pressure was too long. More than 1.38 MPa storage modulus at 200°C was needed for a crack-free Sn-58Bi solder joint morphology for a conventional TC bonding.

Acknowledgements

Conflict of interest

The authors declare no conflict of interest.

Author details

Shuye Zhang[1*], Tiesong Lin[1], Peng He[1*] and Kyung-Wook Paik[2]

1 State Key Laboratory of Advanced Welding and Joining, Harbin Institute of Technology, Harbin, China

2 Department of Materials Science and Engineering, KAIST, Daejeon, South Korea

*Address all correspondence to: syzhang@hit.edu.cn; hithepeng@hit.edu.cn

IntechOpen

References

[1] Stoppa M, Chiolerio A. Wearable electronics and smart textiles: A critical review. Sensors. 2014;**14**(7):11957-11992

[2] Ladner RE. Communication technologies for people with sensory disabilities. Proceedings of the IEEE. 2012;**100**(4):957-973

[3] Zhang S, Kim SH, Kim TW, et al. A study on the solder ball size and content effects of solder ACFs for flex-on-board assembly applications using ultrasonic bonding. IEEE Transactions on Components Packaging & Manufacturing Technology. 2015;**5**(1): 9-14

[4] Sjoberg J, Geiger DA, Shangguan D. Process development and reliability evaluation for inline Package-on-Package (pop) assembly. Electronic Components and Technology Conference, ECTC 2008. 58th. IEEE; 2008:2005-2010

[5] Zhang S et al. Mechanism of solder joint cracks in anisotropic conductive films bonding and solutions: Delaying hot-Bar lift-up time and adding silica fillers. Metals. 2018;**8**(1):42

[6] Jung KS et al. Anisotropic conductive film forming composition. U.S. Patent No. 7,700,007. Ap. 20, 2010

[7] Kim S-C, Kim Y-H. Flip chip bonding with anisotropic conductive film (ACF) and nonconductive adhesive (NCA). Current Applied Physics. 2013;**13**:S14-S25

[8] Liu J, Salmela O, Sarkka J, et al. Reliability of microtechnology: Interconnects, devices and systems. Springer Science & Business Media. 2011

[9] Zhang S, Park JH, Paik KW. Joint morphologies and failure mechanisms of anisotropic conductive films (ACFs) during a power handling capability test for flex-on-board applications. IEEE Transactions on Components Packaging & Manufacturing Technology. 2016;**99**: 1-7

[10] Zhang S, Paik KW. A study on the failure mechanism and enhanced reliability of Sn58Bi solder anisotropic conductive film joints in a pressure cooker test due to polymer viscoelastic properties and hydroswelling. IEEE Transactions on Components Packaging & Manufacturing Technology. 2016; **6**(2):216-223

[11] Kim SH, Choi Y, Kim Y, Paik KW. Flux function added solder anisotropic conductive films (ACFs) for high power and fine pitch assemblies. In: Proceedings of the Electronic Components and Technology Conference (ECTC), 2013 IEEE, Las Vegas, NV, USA. May 28–31, 2013. pp. 1713-1716

[12] Lee K, Saarinen IJ, Pykari L, Paik KW. High power and high reliability flex-on-board assembly using solder anisotropic conductive films combined with ultrasonic bonding technique. IEEE Transactions on Components, Packaging and Manufacturing Technology. 2011;**1**: 1901-1907

[13] Zhang S, Yang M, Wu Y, et al. A study on the optimization of anisotropic conductive films for Sn-3Ag–0.5Cu-based flex-on-board application at a 250°C bonding temperature. IEEE Transactions on Components Packaging and Manufacturing Technology. 2018;**8** (3):383-391

[14] Kim YS, Lee K, Paik KW. Effects of ACF bonding parameters on ACF joint characteristics for high-speed bonding using ultrasonic bonding method. IEEE Transactions on Components Packaging & Manufacturing Technology. 2013; **3**(1):177-182

[15] Keller A et al. Fast-curing epoxy polymers with silica nanoparticles: Properties and rheo-kinetic modelling. Journal of Materials Science. 2016;**51**(1): 236-251

[16] Zhang S et al. A study on the bonding conditions and nonconductive filler contents on cationic epoxy-based Sn-58Bi solder ACFs joints for reliable flex-on-board applications. IEEE Transactions on Components Packaging & Manufacturing Technology. 2017;**99**: 1-8

[17] Zhang S et al. Effects of acrylic adhesives property and optimized bonding parameters on Sn58Bi solder joint morphology for flex-on-board assembly. Microelectronics Reliability. 2017;**78**:181-189

[18] Kim Y-S, Zhang S, Paik K-W. Highly reliable solder ACFs FOB (flex-on-board) interconnection using ultrasonic bonding. Journal of the Microelectronics and Packaging Society. 2015;**22**(1):35-41

[19] Zeng K, Tu KN. Six cases of reliability study of Pb-free solder joints in electronic packaging technology. Materials Science and Engineering: R: Reports. 2002;**38**(2):55-105

[20] LoVasco F, Oien M A. Process for controlling solder joint geometry when surface mounting a leadless integrated circuit package on a substrate. U.S. Patent 4,878,611 [P]. Nov 7, 1989

[21] Teh PL, Mariatti M, Akil HM, et al. The properties of epoxy resin coated silica fillers composites. Materials Letters. 2007;**61**(11–12):2156-2158

[22] Sangermano M, Malucelli G, Amerio E, et al. Photopolymerization of epoxy coatings containing silica nanoparticles. Progress in Organic Coatings. 2005; **54**(2):134-138

[23] Douce J, Boilot JP, Biteau J, et al. Effect of filler size and surface condition of nano-sized silica particles in polysiloxane coatings. Thin Solid Films. 2004;**466**(1–2):114-122

[24] Zhang S, Paik KW. The Effect of Polymer Rebound on Sn-Bi58 Solder ACFs Joints Cracks during a Thermo-Compression Bonding. In: IEEE 67th Electronic Components and Technology Conference (ECTC). IEEE. 2017:2047-2053

[25] Lee K, Kim HJ, Yim MJ, et al. Ultrasonic bonding using anisotropic conductive films (ACFs) for flip chip interconnection. IEEE Transactions on Electronics Packaging Manufacturing. 2009;**32**(4):241-247

[26] Lee K, Oh S, Saarinen IJ, et al. High-speed flex-on-board assembly method using anisotropic conductive films (ACFs) combined with room temperature ultrasonic (US) bonding for high-density module interconnection in mobile phones. Electronic Components and Technology Conference (ECTC). IEEE 61st. IEEE, 2011:530-536

[27] Lee S-H et al. Study on fine pitch flex-on-flex assembly using nanofiber/ solder anisotropic conductive film and ultrasonic bonding method. IEEE Transactions on Components, Packaging and Manufacturing Technology. 2012;**2**.12:2108-2114

[28] Sadeghinia M, Jansen KMB, Ernst LJ. Characterization and modeling the thermo-mechanical cure-dependent properties of epoxy molding compound. International Journal of Adhesion and Adhesives. 2012;**32**:82-88

[29] Suganuma K. Advances in lead-free electronics soldering. Current Opinion in Solid State and Materials Science. 2001;**5**(1):55-64

[30] Kang SK, Sarkhel AK. Lead (Pb)-free solders for electronic packaging. Journal of Electronic Materials. 1994; **23**(8):701-707

[31] Skoog DA, Holler FJ, Crouch SR.
Principles of instrumental analysis.
Cengage learning. 2017

[32] Myung W-R, Kim Y, Jung S-B.
Mechanical property of the epoxy-
contained Sn-58Bi solder with OSP
surface finish. Journal of Alloys and
Compounds. 2014;**615**:S411-S417

[33] Crosby AJ et al. Deformation and
failure modes of adhesively bonded
elastic layers. Journal of Applied
Physics. 2000;**88**(5):2956-2966.
CrossRef. Web

[34] Ferry JD, Myers HS. Viscoelastic
properties of polymers. Journal of the
Electrochemical Society. 1961;**108**(7):
142C. DOI: 10.1149/1.2428174

[35] Chen L et al. The effects of underfill
and its material models on
thermomechanical behaviors of a flip
chip package. IEEE Transactions on
Advanced Packaging. 2001;**24**(1):17-24.
CrossRef. Web